Biosensors and Bioelectronics 45 (2013) 245–251

Contents lists available at SciVerse ScienceDirect

Biosensors and Bioelectronics

journal homepage: www.elsevier.com/locate/bios

Silicon multi-nanochannel FETs to improve device uniformity/stability and femtomolar detection of insulin in serum

Suresh Regonda [a,b], Ruhai Tian [b], Jinming Gao [c], Serena Greene [d], Jiahuan Ding [d], Walter Hu [b,*]

[a] Department of Physics, University of Texas at Dallas Richardson, TX 75080, USA
[b] Department of Electrical Engineering, University of Texas at Dallas Richardson, TX 75080, USA
[c] Department of Chemistry, University of Texas at Dallas Richardson, TX 75080, USA
[d] Diagtronix Inc., Richardson, TX 75080, USA

ARTICLE INFO

Article history:
Received 17 October 2012
Received in revised form
23 December 2012
Accepted 15 January 2013
Available online 21 February 2013

Keywords:
Si nanograting
Bio-FETs
Biosensor
Nanowire
pH sensing
Insulin
Diabetes

ABSTRACT

Here we demonstrate the use of multiple Si nanochannel (NC) or nanograting (NG) instead of the conventional single nanochannel or nanowire design in biosensors. The NG devices can significantly reduce device-to-device variation, and improve device performance, e.g. higher current, higher ON/OFF ratio, smaller subthreshold slope, lower threshold voltage V_t in buffer solution. NG devices also result in higher sensor stability in buffer and diluted human serum. We believe such improvements are due to reduced discrete dopant fluctuation in the Si nanowires and biochemical noise in the solution because of the multiple-channel design. The improved devices allow us to sense pH linearly with 3-aminopropyltriethoxysilane coated devices, and to selectively detect insulin with limit of detection down to 10 fM in both buffer solution and diluted human serum without pre-purification.

Published by Elsevier B.V.

1. Introduction

Driven by the significant progress in nanostructure research, there has been a rapid growth in the field of biosensing utilizing nanostructures as sensing elements, which is critical for a variety of applications in health care, drug delivery, food safety, homeland security, and bioterrorism defense. In spite of different sensing mechanisms these nanoscale biosensors have been operated, the ability to detect molecules at low abundance expeditiously made these nanoscale biosensors highly promising (Besteman et al., 2003; Cui et al., 2001; Elibol et al., 2003; Kong et al., 2000; Stern et al., 2007a). Among many types of sensing technologies, Si nanowire field effect transistors (SiNW-FETs) have emerged as a promising label-free ultrasensitive biosensor platform (Patolsky et al., 2006; Stern et al., 2008) due to their high surface to volume ratio, comparable size to biological molecules and manufacturability with current CMOS technologies (Elibol et al., 2003; Li et al., 2004; Stern et al., 2008; Tian et al., 2011). Fabrication of SiNWs with smaller dimensions is essential to achieve low limit of detection, i.e., high sensitivity, and possibly down to single-to-few molecule detections. The high sensitivity can possibly enable early diagnosis by detecting biomarkers at low concentrations at the early stages of some diseases. CVD methods excel at producing very small NWs, but lacks control over uniformity from device to device, and it is difficult to achieve precise positioning of nanowires and alignment on surfaces for device integration (Cui et al., 2001; Patolsky and Lieber, 2005; Teo and Sun, 2007). Recently, top down lithography has shown capability to produce nanowires with similar or even smaller size than CVD (Trivedi et al., 2011). Lithographic fabrication is advantageous as it offers greater accuracy, uniformity, and patterning flexibility (Chen et al., 2006; Elibol et al., 2003; Gao et al., 2007; Li et al., 2004; Stern et al., 2007a).

In addition to the size of Si nanowires and its fabrication, simulation and experiments have shown that high sensitivity typically requires low doping in the NW channels (Masood et al., 2010; Nair and Alam, 2007; Patolsky et al., 2006), which is also verified experimentally (Gao et al., 2010; Stern et al., 2007a). However, at the low doping conditions, the number of impurity dopants in the tiny volume of nanowires becomes very small and their distribution becomes discrete and non-uniform. The gate control on these randomly arranged dopants is different from wire to wire which result in variation in the device performance (Bonab et al., 2009), which is known as discrete dopant fluctuation in MOSFET devices (Asenov et al., 2003; Mizuno et al., 1994;

* Corresponding author.
E-mail address: Walter.Hu@Utdallas.edu (W. Hu).

0956-5663/$ - see front matter Published by Elsevier B.V.
http://dx.doi.org/10.1016/j.bios.2013.01.027

Nair and Alam, 2007; Vasileska et al., 1998). We recently found that this effect can cause variation and instability in SiNW biosensors (Tian et al., 2011). Although very low limits of detection have been demonstrated using single wire Si NW-FETs (Cui et al., 2001; Kim et al., 2007; Stern et al., 2007a), reliable sensing is still challenging due to the unreliable device performance such as device instability during sensing and large device-to-device variations. For practical applications such as disease diagnostics, uniform and reliable sensors are required to deal with complex biological samples such as blood, serum, urine, and saliva.

Here we present a solution to address the above-mentioned challenge of the SiNW biosensors. By using multiple-nanochannel or nanograting as sensing elements rather than conventional single channel such as NW-FETs, we demonstrate the sensing of pH and protein with greatly improved device uniformity and stability. These Si nano-gratings (SiNG-FETs) with highly uniform performance were fabricated using a CMOS process on a low p-doped silicon-on-insulator (SOI) wafers. The use of a Si nanograting design significantly reduces the device-to-device variation due to reduced discrete doping effects. On the same chip fabricated using the same CMOS process, SiNG-FETs show higher current, higher ON/OFF ratio, sharper subthreshold swing (SS), lower threshold voltage (V_t) in buffer solution, and provide better device stability for biosensing, in comparison to single SiNW devices. These NG-FETs have shown higher sensor stability when they are exposed to buffer solution of high ion concentration for over tens of hours without losing its reproducibility in pH sensing. With these improved devices, selective detection of insulin-analog in both buffer and diluted human serum with a limit of detection (LOD) down to 10 fM is achieved repeatedly.

2. Experimental methods

2.1. Materials and chemicals

Chemicals that were employed in SiNG surface modification such as aminopropyltriethoxysilane (APTES) and 11-(triethoxysilyl) undecanal (TESU) were purchased from Sigma-Aldrich. Sodium cyanoborohydride ($NaBH_3CN$) was purchased from Fluka. The antibody insulin analog lantus used for antibody immobilization was purchased from Sanofi Aventis. The clinical samples used for the insulin detection were provided by Diagtronix Inc.

2.2. Si NG-FET fabrication

Uniform and high performance devices are essential for reliable sensing results. We used silicon nano-gratings (SiNGs) as sensing elements instead of conventional single NW and employed a set of techniques including two-step Si etching, surface thermal oxidation and post-annealing treatment to achieve high performance SiNG-FETs. SiNG-FETs used in this study were fabricated from p-type SOI substrates with a low doping concentration of boron at $10^{15}/cm^3$ with 145 nm thick buried oxide (BOX). A brief schematic of device fabrication process is shown in the Supporting information (Fig. S1a). Photolithography and Cl_2 plasma etching were applied to define active device area and source drain contact pads. Ion implantation with phosphorous or boron (10^{19} cm^{-3}) was used to form source drain junctions for NMOS and PMOS respectively. Then, we used e-beam lithography (EBL) with hydrogen silses quioxane (HSQ—Dow Corning Co.) as a negative tone inorganic e-beam resist (Grigorescu et al., 2007; Regonda et al., 2008) to define the Si nanochannels. EBL with 30 keV beam energy and 250 pA beam current was performed on a Zeiss Supra 40 scanning electron microscopy (SEM) with a Nabity pattern generator. HSQ was developed in 25 wt% tetramethyl-ammonium-hydroxide (TMAH) for 60 s at a temperature of 40 °C. E-beam exposed HSQ can act as etch mask for pattern transfer to the top Si layer of the SOI wafer. However, after the Si is etched, it becomes difficult to remove the cured HSQ without etching the underlying BOX. Direct stripping of HSQ using buffered oxide etchant (BOE) will also dissolves the buried oxide resulting in unreliable floating Si nanolines (Fig. S2a). To address this issue, a two-step Si etch process was developed (Fig. S2b). After patterning and development of HSQ nanolines, plasma etching with Cl_2 chemistry was used to partially etch the top Si layer. This first step of etch process left about 30 nm of Si on top of the buried oxide untouched. Then the HSQ on the top of Si was removed using BOE. This process prevents etching of underlying BOX from BOE wet etch having left over (~30 nm) Si as a protecting layer. Once the HSQ was stripped, a second plasma etch process with the same Cl_2 gas recipe was applied to achieve the complete transferring of nanowires to Si by etching remaining Si. This approach not only allows us to get sub 50 nm wide but also thinner Si NWs, which is advantageous for biosensing experiments as it improves detection sensitivity (Elfstrom and Linnros, 2008; Xinrong Yang et al., 2012). An SEM image of stable and uniform SiNGs are shown in Fig. S2b.

After the Si nanogratings are formed, oxidation process was performed on the SiNG-based devices at 900° C in O_2 ambient to form a 3–6 nm SiO_2 layer as gate dielectrics. Then the devices were annealed in forming gas at 450 °C after metal contacts are made to improve the ohmic contacts between metal and doped S/D pads. We observed that the oxidation and annealing process can also reduce surface charges and Si dangling bonds that are induced during the device fabrication, resulting in improved device stability. Finally, the area other than SiNGs was passivated by silicon nitride (Si_3N4). An optical image of a finished SiNG-FET, with multi-nanowires connecting the doped source/drain pads was shown in Fig. 1a. Fig. 1b shows an electron micrograph of 50 nm wide, 30 nm thick, and 20 μm long Si nanochannels. Fig. 1c illustrates (not drawn to scale) the SiNG FET architecture and biasing setup for biosensing experiments.

Typical current–voltage (I–V) characteristics of n-type Si-NGFETs with different number of nanochannels at room temperature are shown in Fig. 2. During the electronic characterization of the device, a reference electrode Ag/AgCl wire was used as solution gate to bias Si-NGs in the solution. Drain current I_{ds} as a function of reference gate voltage V_{ref} at a drain voltage V_{ds} of 100 mV in 0.5 mM K–PBS solution (pH~8.2) is plotted in a logarithmic scale in Fig. 2a. These devices with 100 NCs connecting source and drain have shown uniform and good performance with ON/OFF~10^6, SS of ~80 mV/dec, and V_t of ~1 V. The gate leakage currents is low (pico amps) due to the protection of to the gate dielectrics and BOX layer.

2.3. SiNG surface modification with self-assembly monolayer for pH sensing

Before surface functionalizon, the Si-NG area was first treated with piranha for 30 s and followed by rinsing with deionized water copiously and blown dry with nitrogen. This piranha clean is necessary to obtain a clean and hydroxy terminated SiO_2 surface covering the Si-NG devices. After the piranha clean the Si-NG surface was first chemically modified with 1% APTES in anhydrous ethanol for 30 min followed by rinsing with absolute ethyl alcohol, and blown-dry with nitrogen. This silanation process converting the silonal groups on the Si-NG surface into amines terminated surface. After blown-dry with nitrogen, the samples were baked at 120 °C for 20 min and ready for pH sensing experiments.

2.4. Anti-insulin immobilization for protein detection

A detailed surface functionalization process for antibody immobilization is illustrated schematically in Fig S3. Before surface functionalizon, the SiNG-FETs were first treated with piranha for 30 s and followed by rinsing with deionized water copiously and blown dry with nitrogen. Then, the SiNGs were reacted in 0.1% 11-triethoxysilundecanal in 98% anhydrous toulene solution for 1.5 h. After this, the chips were rinsed with excess mounts of anhydrous toulene and dried with N_2. The aldehyde functionalized chip was exposed to 0.1 mL anti-insulin solution (50 μg/mL) in 0.25 mM K–PBS (diluted from ~100 mM KCl and KH_2PO_4 in original K–PBS) based buffer solution with pH 8.4 containing 0.5 mM sodium cyanoborohydride ($NaBH_3CN$) for 4.5 h. The anti-insulin immbolized sample was washed with plenty of K–PBS buffer solution. Later, the unreacted aldehyde groups were passiavted by using 5 mM ethanolamine containing 0.5 mM $NaBH_3CN$ in 0.25 mM K–PBS buffer solution with pH (7.4) for 3 h to avoid non-specific binding to the surface. To test the ultimate sensitivity of detecting the target molecules, we used buffer solutions of relatively low salt concentration e.g., 0.25 mM K–PBS, to obtain sufficiently long Debye length (> 30 nm) to avoid shielding effects (Stern et al., 2007b).

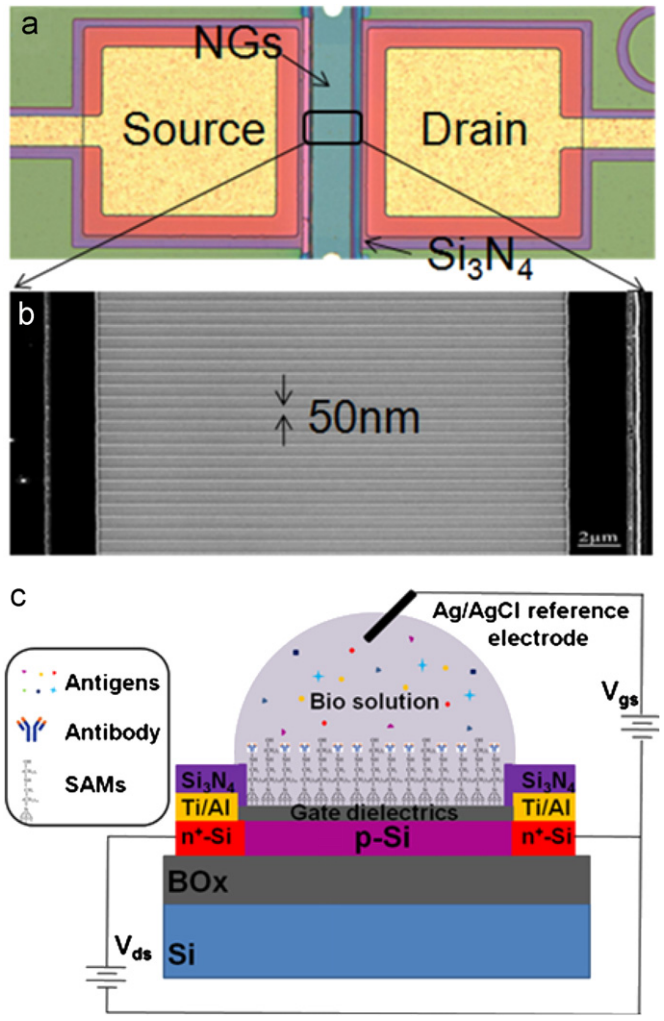

Fig. 1. (a) Optical image of NG-FETs with 100 nanochannels with (b) SEM zoom-in view of nanochannels (W=50 nm, t=30 nm, L=20 μm) connecting highly doped source/drain pads. (c) Cross-sectional illustration of chemically constructed SiNG FET biosensor with Ag/AgCl reference electrode suspended in the analyte-bearing S/D channel platform (not drawn to scale).

3. Results and discussions

3.1. Impact of the number of nanochannels

To obtain accurate and meaningful biosensing results, it is important to have reliable and uniform Si bio-FETs with high device performance. It is a well known fact that the discrete dopant fluctuations affect device reliability due to the small number of dopants in the nanochannels. In our devices, the total number of dopants in each 20 μm long nanochannel is about 30. The distribution of these dopants in the 20 μm long nanochannel can be significantly non-uniform for different devices (causing varied scattering of electron and device current), leading to variation of device performance and biosensing results. To study this effect, we made an array of 10 devices on the same chip for each type of devices and measure their I–V curves and extract their characteristics.

Fig. 2 shows a typical performance characterisitcs (I_{ds}–V_{gs}) and (I_{ds}–V_{ds}) of n-type SiNG-FETs with different numbers of nanochannels (100, 10, and 1), 20 μm in length, 50 nm in width, and 30 nm in height fabicated on the same chip using the same process. Measurements were carried out in 0.5 mM K–PBS solution using a Ag/AgCl wire as the solution gate. I–V curves in Fig. 2a show that the device current monotonically scales with the number of nanochannels. Additionally, devices with 100 NCs show higher ON/OFF ratio with three orders in magnitude, four times smaller SS, and lower V_t in buffer solution compared to single channel devices. Fig. 2b represents the I_{ds}–V_{ds} characteristics of 100 nanochannels, demonstrating

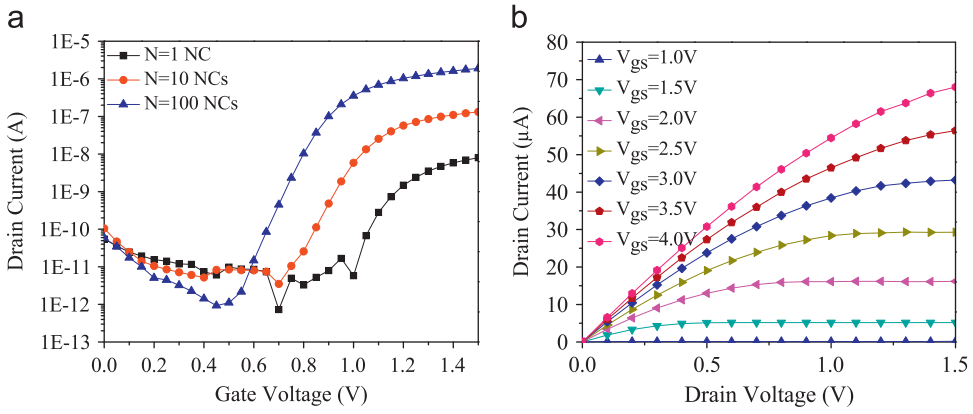

Fig. 2. Comparison of device characteristics of SiNG-FETS with different numbers of NCs: (a) I_d–V_g, (b) I_d–V_d of 100 NCs measured in 0.5 mM K–PBS solution.

Table 1
Device parameters and their variation extracted from *I–V* curves of n-type NG-FETs (5–10 devices averaged for each kind of devices on the same chip).

# Of NCs	Device parameters: value (left) and variation (right)						
	$G_{m\ max}$ (nS)	G_m (%)	V_t (V)	V_t (%)	SS (mV/dec)	SS (%)	I_{on}/I_{off}
100	3275.7 ± 221.47	6.76	0.86 ± 0.015	1.8	65.10 ± 3.08	4.73	$\sim 10^6$
10	253.42 ± 118.83	46.89	1.02 ± 0.06	6.1	74.07 ± 7.12	9.61	$\sim 10^4$
1	12.6 ± 11.08	87.74	1.15 ± 0.16	14	231.35 ± 155.6	67.28	$\sim 10^3$

good device characteristics. The high drive current of nanograting devices in buffer solution can improve signal to noise ratio and reduce the complexity of read out circuits, as small signals such require more advanced amplifiers and filters.

Table 1 summarizes the measured and extracted device parameters (V_t, SS, G_m) from the *I–V* curves of the SiNG-FETs with 100, 10, and 1 nanochannels. The presented data is the average value of five to ten devices for each type of devices on the same chip (a few devices close to chip edge did not work). For each device parameter listed in the table, the values on the left and the right represent the average value and the percentage variation from device to device, respectively. Subthreshold swing for the NG devices was extracted from the *I–V* curve and found to be smaller than 75 mV/dec with the smallest value of 63 mV/dec. This value is close to the theoretical limits (60 mV/dec), indicating a good interface between the oxide and the Si nanochannel (Sze, 2007). This small SS can be attributed to our long channel design and reduced interface charge density due to oxidation and post anneal treatments. Small SS is desirable for high sensitivity since the carriers in the NW possess extended Debye length in the subthreshold regime where maximum sensitivity can be possible due to the gating of the surface charges on the whole NW (Gao et al., 2010). These devices exhibit high ON/OFF ratio ($>10^6$) and low off state currents (pico amps). The reason for this excellent switch-off behavior may be due to the reduced the electron concentration (Henschel et al., 2004) at the side walls and also smooth edges of the SiNW due to the oxidation process. The subthreshold region with low subthreshold currents shows the sharp dependence of drain currents with gate bias (Sze, 2007).

Most importantly, the results in Table 1 show that devices with 100 NCs have significantly less variation of V_t ($\sim$2%), SS ($\sim$5%), and maximum transconductance (G_m) ($\sim$7%) than those with single NWs ($V_t \sim 14\%$, SS$\sim$67%, $G_m \sim 88\%$ variations respectively). The physcial dimensions of the nanowires were examined in SEM and shows high size uniformity. Device-to-device variations of all device characteristics decrease monotonically with increase of channel numbers, clearly showing that the multichannel design can efffectively reduce random dopant effects on device uniformity. We also note that these variations are significantly smaller compared to the previous work related to single NW devices either by CVD grown, e.g. $\sim$2 V variation in V_t (Patolsky and Lieber, 2005) or lithographic approaches (Elfstrom et al., 2007).

3.2. Electrochemical passivation

Our experiments show that the device performance and stability depend on both the number of nanowires as well as on the sensor passivation. To eliminate an electrochemical reaction of the metal contacts with buffer solutions and improve the sensitivity, passivation of the surrounding area of SiNG-FETs is necessary to get stable device performance in liquid environment (Stern et al., 2007b). Previously, epoxy based photoresist SU8 or silicon nitride (Si_3N_4) have been used as the passivation layers (Ashcroft et al., 2004; Gould and Awan, 2003; Hirohata et al., 1994). Here we compared these two passivation materials in terms of their effects on sensor stability and performance. SU8 channels with a thickness of 13 μm were patterned by photolithography. Si_3N_4 channels with a thickness of 150 nm were sputtered by RF magnetron using a Si target in presence of Ar and N_2 as process and reacting gases (Vila et al., 2004; Zambom et al., 2009). The stabilities of device with these two different passivation materials in buffer solution (1 mM of NaCl, 1 mM PBS, pH 7.4) were studied. The measurements were carried out in a wet ambient where SiNGs were immersed in a fluidic bath of buffer solution and a fixed gate voltage is applied through the Ag/AgCl reference electrode. After the measurements, the chip was rinsed with DI water, dried by baking at 120 °C for 15 min, and the measured in air (dry ambient) using the back gate on the bottom Si substrate. This set of experiments, in wet and dry ambient was repeated several times to investigate the quality of electrochemical passivation of devices, and the device *I–V* curves are plotted in Fig S4a and b for both Si_3N_4 and SU8 passivated devices respectively. The results indicate that SiNG-FET performs better in wet ambient, e.g. much lower V_t, which is due to the thinner dielectric layer (3–6 nm) using solution gate vs. using back gate (145 nm BOX is used as the dielectric layer). The devices may also benefit from the passivation of active defects due to the diffusion of the ions in the buffer solution to the channel interface (Lin et al., 2007). The reduced V_t of devices allows the use of lower gate voltage, preventing possible electrochemical reaction on the device surfaces. The SU8 passivated devices show poor performances in both dry and wet conditions compared to the Si_3N_4 passivated devices, indicating SiN is a better passivation material likely due to the dense structure of sputtered silicon nitride preventing the penetration of ions (Na^+ or K^+) into the BOX (Plummer, 2000). The Si_3N_4 layer is also an ideal passivation material due to its inert to harsh chemical conditions such as piranha which are used to clean the SiNW surface before antibody coating in our experiments.

3.3. Device stability in buffer solutions

In applications requiring continuous monitoring for extended periods (hours, as in many clinical applications) (Bergveld and Sibbald, 1988), device electrical stability in buffers and biologic fluids is critical. Here we investigated the time dependent stability of device in different pH buffer solutions. We examined our SiNG-FETs by exposing them to buffer solutions of relatively high salt concentrations (10 mM Tris, 100 mM KCl) at different pH values of 5, 7, and 9, for a long duration of time after coating the sensor area with self assembled monolayer of APTES. Fig. 3a shows the device drain current vs. time for repeated cycles of buffer solutions of three different pH (5, 7, and 9) for 8000 s, showing a good reproducibility and stability of SiNG-FET with 10 NCs more than 20 h, while single NWs do not yield such repeabiltiy (Tian et al., 2011). We believe that this long term stability and reproducibility was achieved mainly due to the following reasons: (1) multiple NCs as sensing elements instead of single channel, (2) SAM coating, and (3) passivation by means of Si_3N_4 sheilding from ion diffusion and device degradation.

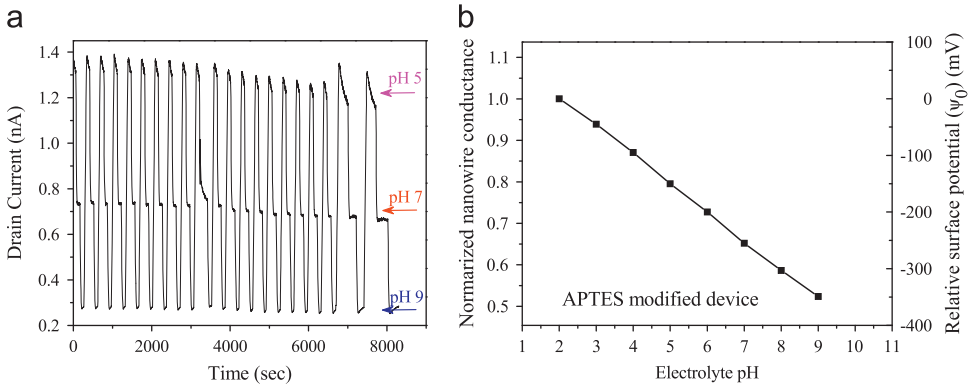

Fig. 3. (a) Real-time current response of the SiNG-FET (NC=10) to the three different pHs (5, 7, and 9) at highly concentrated buffer solution (10 mM Tris, 100 mM KCl) shows good stability and reproducibility for 8000 s. (b) The normalized device conductance (left *y*-axis) and the relative device surface potential (right *y*-axis) vs. solution pH values.

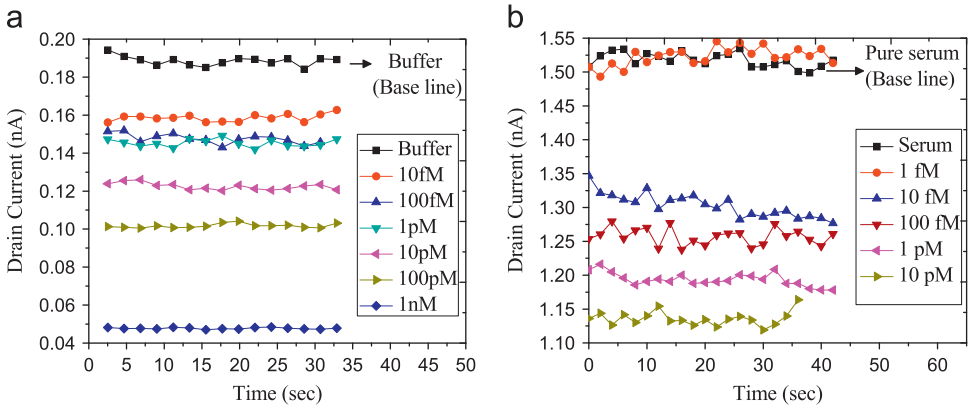

Fig. 4. Measured current levels of SiNG-FETs with 100 nanochannels conjugated with anti-insulin for (a) buffer solutions of different insulin concentration from 10 fM to 1 nM (b) diluted serum solution with added insulin concentration from 1 fM to 10 pM. (For interpretation of the references to color in this figure, the reader is referred to the web version of this article.)

To demonstrate these devices are versatile for sensing surface charges, we first studied the pH sensing for a wide range of 2–9. We used a flow-through microfludic system to deliver solutions with different pH. To control the variations in ion concentration at different pH values the buffer solutions are maintained at a relatively high salt concentration (10 mM PBS, 0.1 M NaCl) to eliminate the stream potential effect, which might be caused by different pH (Dong et al., 2009). Response of SiNG-FET with 100 NCs when exposed to buffer solutions of different pH values is shown in Fig. 3b. We observed a linear response of the drain current (left *y*-axis) with pH values ranging from 2.0 to 9.0 when SiNW surface chemically modified with APTES. The mechanism of ion sensitive FETs or bio-FETs response to ions has been intensively discussed in the literature (Bergveld, 2003; Kargar, 2009; Nair and Alam, 2008; Siu and Cobbold, 1979; Yates et al., 1974). The linearity of the surface potential (Fung et al., 1986) with respect to the pH value depends on the pK_a value of the material coated on the NG surface. Also, the relative surface potential changes $\Delta\Psi$ (reference to data point at pH 2.0 were extracted from the I_d–V_g and I_d–pH curves) (Tian et al., 2011), were shown in Fig. 3b on the right hand side of the vertical axis with respect to the different pH values. It clearly indicates the linear correlation between surface potential and ΔpH (~50 mV/pH) for APTES coated surfaces (Golub et al., 1996). We believe that these prominent pH sensing results are due to the good SAM coverage and stable SiNG-FETs under buffer conditions. This confirms us that SiNG-FETs are reliable platforms for sensing surface charge.

3.4. Detection of insulin-analog

Insulin is a diabetes related hormone and the quick detection of its level in blood is important for diabetes mellitus studies, diagnosis and also guiding its treatment. After anchoring the antibodies (anti-insulin) on the surface of SiNG-FET biosensor, buffer solutions (0.25 mM K–PBS) containing varied insulin concentration from 1 fM to 1 nM were applied to the sensor and the device current levels were measured, as shown in Fig. 4a. The black curve (reference current level) represents pure buffer with no added insulin. When 10 fM insulin was introduced, a significant change (0.2 nA) in the current (red curve) was observed, indicating the detection limit is around 10 fM or lower. Higher insulin concentration yields higher change of current level from the baseline, representing a monotonic dependence of current change with insulin concentration.

To study sensing specificity and test if the sensors can work using physiological samples, we did the sensing experiments using human serum samples from two patients. The serum samples were diluted by 10,000× by the same buffer (0.25 mM K–PBS) to reduce its salt concentrations to achieve sensitivity that can be comparable to buffer study in Fig. 4. 10 fM to 0.1 nM of insulin were then added to the serum samples. These serum samples do not contain insultin ($\ll$10 fM after dilution) with careful patient care before collect their samples, and therefore they can be used as negative control, yielding a baseline reference current level for the sensor. Similar sensing results are shown in Fig. 4b.

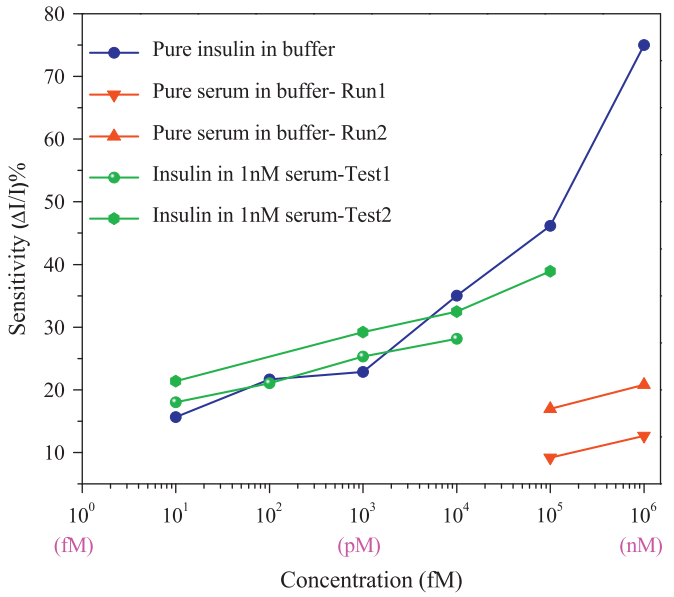

Fig. 5. Logarithmic representation of sensitivity vs. insulin concentration in buffer solution (blue) and diluted serum (green) in the range of 10 fM to 1 nM concentrations. Red curves are the signals from non-specific binding from high concentrations of serum proteins in the same diluted serum without adding insulin. (For interpretation of the references to color in this figure legend, the reader is referred to the web version of this article.)

The sensitivty of the detection is defined as the percentage change in the current (normalized for different devices that may have different currents) at the presence of the specific insulin concentration, which is plotted in Fig. 5 for sensing results in both buffer and diluted human serum. Both buffer and two patient serum samples show a monotonic increase of sensitivity over increased insulin concentration. Sensing results for serum samples and buffer samples match relatively well in the range of 10 fM to 100 pM. The limit of detection is about 10 fM. It is encouraging that the patient samples did not cause false positives although the overall concentration of over 4000 types of proteins Shen et al., 2005 in the serum is high (even after dilution). The red curve in Fig. 5 is the signals from non-specific binding from diluted serum. The detection range is approximately five orders of magnitude with good selectivity over diluted serum. The sensor is stable in serum for repeated multiple tests over the period of a week, showing good stability.

4. Conclusions

To summarize, here we have demonstrated the high performance of low doped SiNG-FETs fabricated using a CMOS compatible process. The key finding of our study is that the number of nanochannel has strong impact on device performance, device-to-device variation, and biosensing stability. We found that nanogratings compared to single nanochannel designs resulted in higher ON/OFF ratio, smaller SS, lower V_t, and importantly, higher stability with a significant reduction in device to device variation. We believe such improvements are due to minimized discrete dopant fluctuations and interference from the biosensing environment. Using SiNG-FETs with improved device performance, we demonstrate the sensing pH linearly with APTES coated devices, and selective detection of insulin with limit of detection down to 10 fM in both buffer and diluted human serum without purification.

Acknowledgments

This work is supported by National Science Foundation (ECCS-0955027, CBET #1064574, and IIP # 1127761), Texas Instruments Inc., and Texas Medical Consortium. This research project was also partially funded by Diagtronix, Inc. Walter Hu is the principal investigator for this research project and has a significant financial interest in Diagtronix, Inc. This financial interest has been disclosed to UT Dallas and a conflict of interest management plan is in place to manage the potential conflict of interest associated with this research program. Suresh Regonda would like to thank Krutarth Trivedi for his contribution in setting up microfluidic system and useful discussions.

Appendix A. Supplementary information

Supplementary data associated with this article can be found in the online version at http://dx.doi.org/10.1016/j.bios.2013.01.027.

References

Asenov, A., Brown, A.R., Davies, J.H., Kaya, S., Slavcheva, G., 2003. IEEE Transactions on Electron Devices 50 (9), 1837–1852.
Ashcroft, B., Takulapalli, B., Yang, J., Laws, G.M., Zhang, H.Q., Tao, N.J., Lindsay, S., Gust, D., Thornton, T.J., 2004. Physica Status Solidi B—Basic Research 241 (10), 2291–2296.
Bergveld, P., 2003. In: Proceedings of the IEEE Sensor Conference Toronto. pp. 1–26.
Bergveld, P., Sibbald, A., 1988. Comprehensive Analytical Chemistry XXIII.
Besteman, K., Lee, J.O., Wiertz, F.G.M., Heering, H.A., Dekker, C., 2003. Nano Letters 3 (6), 727–730.
Bonab, J.A.F., Abtahi, S.E., Hosseini, S.E., 2009. The effects of random distribution fluctuations of dopants on SOI-MOSFET performance. In: Proceedings of the 2009 IEEE International Conference of Electron Devices and Solid-State Circuits. pp. 67–70.
Chen, Y., Wang, X., Erramilli, S., Mohanty, P., Kalinowski, A., 2006. Applied Physics Letters 89 (22), 1–3.
Cui, Y., Wei, Q.Q., Park, H.K., Lieber, C.M., 2001. Science 293 (5533), 1289–1292.
Dong, Rip, Kim, C.H.L., Xiaolin, Zheng, 2009. Nano Letters 9 (5), 1984–1988.
Elfstrom, N., Juhasz, R., Sychugov, I., Engfeldt, T., Karlstrom, A.E., Linnros, J., 2007. Nano Letters 7, 2608–2612.
Elfstrom, N., Linnros, J., 2008. Nanotechnology 19 (23), 1–5.
Elibol, O.H., Morisette, D., Akin, D., Denton, J.P., Bashir, R., 2003. Applied Physics Letters 83 (22), 4613–4615.
Fung, C.D., Cheung, P.W., Ko, W.H., 1986. IEEE Transactions on Electron Devices 33 (1), 8–18.
Gao, X.P.A., Zheng, G.F., Lieber, C.M., 2010. Nano Letters 10 (2), 547–552.
Gao, Z.Q., Agarwal, A., Trigg, A.D., Singh, N., Fang, C., Tung, C.H., Fan, Y., Buddharaju, K.D., Kong, J.M., 2007. Analytical Chemistry 79 (9), 3291–3297.
Golub, A.A., Zubenko, A.I., Zhmud, B.V., 1996. Journal of Colloid and Interface Science 179 (2), 482–487.
Gould, R.D., Awan, S.A., 2003. Thin Solid Films 433 (1–2), 309–314.
Grigorescu, A.E., van der Krogt, M.C., Hagen, C.W., Kruit, P., 2007. Journal of Vacuum Science & Technology B 25 (6), 1998–2003.
Henschel, W., Wahlbrink, T., Georgiev, Y.M., Lemme, M., Mollenhauer, T., Vratzov, B., Fuchs, A., Kurz, H., Kittler, M., Schwierz, F., 2004. Solid-State Electronics 48 (5), 739–745.
Hirohata, Y., Shimamoto, N., Hino, T., Yamashima, T., Yabe, K., 1994. Thin Solid Films 253 (1–2), 425–429.
Kargar, A., 2009. Chinese Physics Letters 26 (6).
Kim, A., Ah, C.S., Yu, H.Y., Yang, J.H., Baek, I.B., Ahn, C.G., Park, C.W., Jun, M.S., Lee, S., 2007. Applied Physics Letters 91 (10), 1–3.
Kong, J., Franklin, N.R., Zhou, C.W., Chapline, M.G., Peng, S., Cho, K.J., Dai, H.J., 2000. Science 287 (5453), 622–625.
Li, Z., Chen, Y., Li, X., Kamins, T.I., Nauka, K., Williams, R.S., 2004. Nano Letters 4 (2), 245–247.
Lin, H.C., Su, C.J., Hsiao, C.Y., Yang, Y.S., Huang, T.Y., 2007. Applied Physics Letters 91, 20.
Masood, M.N., Chen, S., Carlen, E.T., van den Berg, A., 2010. ACS Applied Materials & Interfaces 2 (12), 3422–3428.
Mizuno, T., Okamura, J., Toriumi, A., 1994. IEEE Transactions on Electron Devices 41 (11), 2216–2221.
Nair, P.R., Alam, M.A., 2007. IEEE Transactions on Electron Devices 54 (12), 3400–3408.
Nair, P.R., Alam, M.A., 2008. Nano Letters 8 (5), 1281–1285.
Patolsky, F., Lieber, C.M., 2005. Materials Today 8 (4), 20–28.
Patolsky, F., Zheng, G.F., Lieber, C.M., 2006. Analytical Chemistry 78 (13), 4260–4269.

Plummer, J.D., 2000. Silicon VLSI technology Fundamentals. Practise and Modeling.
Regonda, S., Aryal, M., Hu, W.C., 2008. Journal of Vacuum Science & Technology B 26 (6), 2247–2251.
Shen, Y., Kim, J., Strittmatter, E.F., Jacobs, J.M., Camp, D.G., Fang, R., Tolié, N., Moore, R.J., Smith, R.D., 2005. Proteomics 5 (15), 4034–4045.
Siu, W.M., Cobbold, R.S.C., 1979. IEEE Transactions on Electron Devices 26 (11), 1805–1815.
Stern, E., Klemic, J.F., Routenberg, D.A., Wyrembak, P.N., Turner-Evans, D.B., Hamilton, A.D., LaVan, D.A., Fahmy, T.M., Reed, M.A., 2007a. Nature 445 (7127), 519–522.
Stern, E., Wagner, R., Sigworth, F.J., Breaker, R., Fahmy, T.M., Reed, M.A., 2007b. Nano Letters 7, 3405–3409.
Stern, E., Vacic, A., Reed, M.A., 2008. IEEE Transactions on Electron Devices 55 (11), 3119–3130.
Sze, S.M., 2007. Physics of Semiconductor Devices, 3rd ed. John Wiley & Sons New York.
Teo, B.K., Sun, X.H., 2007. Chemical Reviews 107 (5), 1454–1532.
Tian, R., Regonda, S., Gao, J., Liu, Y., Hu, W., 2011. Lab on a Chip 11 (11), 1952–1961.
Trivedi, K., Yuk, H., Floresca, H.C., Kim, M.J., Hu, W., 2011. Nano Letters 11 (4), 1412–1417.
Vasileska, D., Gross, W.J., Ferry, D.K., 1998. In: Proceedings of the 1998 Sixth International Workshop on Computational Electronics. pp. 259–226.
Vila, M., Prieto, C., Ramirez, R., 2004. Thin Solid Films 459 (1–2), 195–199.
Xinrong Yang, W., Frensley, Dian, Zhou, Hu, W., 2012. IEEE Transactions on Nanotechnology 11 (3), 501–512.
Yates, D.E., Levine, S., Healy, T.W., 1974. Journal of Chemical Society—Faraday Transactions I 70, 1807–1818.
Zambom, L.D., Mansano, R.D., Mousinho, A.P., 2009. Microelectronics Journal 40 (1), 66–69.